International Journal of Engineering Trends and Technology
ISSN: 2231-5381/ https://doi.org/10.14445/22315381/IJETT-V74I4P107

Volume 74 Issue 4, 87-100, April 2026

Original Article

Precision Food Crop Mapping Using Deep Neural Networks and Improved Dipper Throat Optimization Techniques

Anil Antony[1], Ganesh Kumar R[2]

[1,2]*Department of Computer Science & Engineering, CHRIST (Deemed to be University), School of Engineering and Technology, Kengeri Campus, Bangalore, India.*
[1]*Department of Computer Science and Engineering, Sahrdaya College of Engineering and Technology, Thrissur, Kerala, India.*

[1]*Corresponding Author : anil.antony@res.christuniversity.in*

Received: 19 August 2025 Revised: 23 January 2026 Accepted: 12 February 2026 Published: 29 April 2026

Abstract - *In recent times, the use of Remote Sensing (RS) data obtained from Unmanned Aerial Vehicles (UAVs) has gained significant popularity in crop classification tasks, including crop mapping, yield prediction, and soil classification. The classification of food crops utilizing RS Imageries (RSI) is a major application of RS tools in crop growing. Meeting the conditions for investigating these data requires more difficult approaches, and Artificial Intelligence (AI) technologies offer the mandatory support. Because of the variation and division of crop planting, archetypal classification methods have fewer classification outcomes. This manuscript focuses on the design and execution of a Leveraging Enhanced Dipper Throat Optimization Algorithm with Dipper-Inspired Precision Classification for Remote-sensed Optimized (DIP-CROP) Processing methodology. The drive of the DIP-CROP algorithm is to classify distinct types of crops that exist in remote sensing. At first, the DIP-CROP model applies image processing using the Sobel Filter (SF) to eliminate the noise. Next, the presented DIP-CROP technique takes place SqueezeNet model is employed for the feature extractor. To classify the food crop types, the DIP-CROP approach utilizes a Multi-Head Attention-based Bi-directional Long Short Term Memory (MHA-BiLSTM) algorithm. For hyperparameter tuning of the MHA-BiLSTM classifier, the Enhanced Dipper Throat Optimization Algorithm (EDTOA) will be applied in this work. The optimization process utilizes Levy flight distribution, which is known for its faster convergence due to efficient exploration of the search space. Levy flights can be used to take larger steps in exploration, which prevents getting stuck in local minima and accelerates convergence. The performance of the DIP CROP method is examined experimentally using a benchmark database. Experimental results affirmed the superior solution of the DIP-CROP algorithm over existing methods.*

Keywords - *Food Crop Classification, Remote Sensing, Levy Flight, Feature Extractor, Sobel Filter.*

1. Introduction

Timely and accurate determination of each food crop type is essential for food safety, sustainable agricultural plans, and precision farming. Crop-type data is essential for many decision-making tasks, such as yield prediction, irrigation scheduling, pest management, and policy-making. The population is increasing across the globe, and Climate variability and the structure of land use are changing so rapidly that traditional field-based cropland monitoring methods will become more inefficient, time-consuming, and costly.

Thus, the Remote Sensing (RS) technique, coupled with data-driven models, has become a useful approach for large-scale agricultural monitoring. Food security is the most significant aspect of political stability, sustainable financial growth, and social harmony [1]. A food security evaluation method that can be applied to forecast grain crop harvesting and examine food security difficulties, with higher importance for standardizing food markets, adjusting planting structure, and formulating agricultural strategies [2]. Food security has received massive attention worldwide since 1974. Over recent years, soil desertification, salinization, urbanization, global climate change, and other concerns have negatively influenced food production. At the same time, fluctuating global food prices and a higher population growth rate have further increased the severity of its food security concerns [3]. Some investigations discussed the essentials for a global strategy to guarantee future food security, where agriculture plays an active role. Crops like wheat, corn, barley, and rice are the main food sources in various parts of the world, hence data on their spatial distribution and condition are considerably vital at the national, global level and regional

levels [4]. Accurate and earlier consideration of crop planting alteration, structure, and optimization is based on scientific theories and technologies, which are mainly significant to the viable utilization of resources and promoting reasonable allocation.

The RS for agricultural applications primarily focuses on optical data obtained in the near-infrared and visible parts of the electromagnetic spectrum [5]. Currently, with the development in processing capabilities and sensor technologies, it has become possible to expand scientific methods and usage of new complementary data resources for concurrent investigation of multiple-source data [6]. RS has proven to be an efficient device for monitoring cropping practices [7]. Several investigations have shown that the synergetic usage of several spatial data resources can maximize precision classification [8]. Mainly, the necessity of multiple-sensor data investigation for land and crop type classification is becoming increasingly important, for example, the separation of crop categories that resemble each other in one region, or data resources with frequent cloud cover [9]. High-resolution RSI is widely applied for crop classification. In recent times, Deep Learning (DL) and Machine Learning (ML) methods have become broadly utilized in agriculture, mainly to enhance crop qualities and productivity, and have attained excellent outcomes in cropland mapping [10].

Despite extensive progress in remote sensing-based agricultural monitoring, there are a number of critical gaps associated with existing crop classification frameworks. Most of the previous studies are mainly based on spatial feature extraction approaches with a convolutional neural network or emphasize temporal modeling only, and thus cannot capture the spatial-temporal dependency inherent in crop growth cycles jointly. Although DL methods have been developed to improve the accuracy of classifications, temporal learning with attention is not widely used in UAV-based crop mapping, which is a limitation of the model to effectively learn long-range dependencies among sequential observations.

Furthermore, hyperparameter optimization is most often addressed as an auxiliary post-processing task of the learning process rather than as an integral part of the learning architecture, which results in suboptimal convergence and poor generalization. Existing bio-inspired optimization algorithms also exhibit poor adaptive global exploration, often leading to premature convergence. In addition, many reported studies are not statistically validated, do not provide reproducibility information, and lack the scalability and discussion of real-world deployment, which limits their practical applicability. In order to fill in these gaps, this research proposes a new end-to-end framework called DIP-CROP (Dipper-inspired Precision Classification for Remote-sensed Optimized Processing). The key novelty of the proposed approach lies in unifying the compact spatial feature extraction, attention-driven temporal modeling, and adaptive metaheuristic optimization in a single learning pipeline. Unlike the traditional approaches that use heavy backbone networks, DIP-CROP exploits SqueezeNet to get efficient features with fewer computational overhead, which can be used in UAV-based applications. The introduction of the MHA-BiLSTM network allows the modeling of temporal dependencies from multi-temporal remote sensing data, allowing a better discrimination between crops with similar spectral characteristics. In comparison to the current optimization strategies like Particle Swarm Optimization (PSO), Grey Wolf Optimization (GWO), and Genetic Algorithms, the proposed EDTOA proposes the concept of Levy flight-based stochastic exploration with dynamic step size adaptation. This design allows for wider search across a global region on early iterations and tighter exploitation on local regions on later iterations, allowing for faster convergence and better classification robustness. Moreover, in contrast to previous studies, the proposed framework has a strong emphasis on reproducibility, specifically by being explicit about dataset splits, parameter settings, and implementation strategies, as well as incorporating statistical validation to ensure performance significance.

Compared with the most recent state-of-the-art methods for crop classification using UAVs, DIP-CROP achieves better performance by simultaneously addressing spatial-temporal feature learning, hyperparameter adaptability, and computational efficiency. The thorough evaluation through experiments, including benchmark comparison and statistical analyses, further proves the effectiveness and practicality of the proposed methodology for precision agriculture and large-scale food crop monitoring. The major contribution of this study can be summarized as follows:

- A novel hybrid DL is proposed that includes the integration of SqueezeNet-based compact spatial feature extraction models and Multi-Head Attention-enabled Bidirectional Lstm for successful temporal modeling of remote sensing images acquired from UAVs.
- An improved bio-inspired optimization approach is proposed, named EDTOA, and is based on two motivations of Levy-flight-based stochastic exploration and dynamic scaling in order to reach efficient and robust optimization on hyperparameters.
- A complete reproducible framework for end-to-end crop classification is created that explicitly includes hyperparameter sensitivity, together with reproducibility, achieving the same performance in a variety of experiments related to changing experimental setup.
- An extensive experimental evaluation is performed on the benchmark UAV datasets, with the use of statistical evaluation and comparative analysis with state-of-the-art techniques (classification and optimization) in order to demonstrate the effectiveness of the proposed approach.

2. Literature Survey

In remote sensing, the technology of monitoring agricultural systems over vast areas is being made possible, where the collection of spatial and temporal information is done continuously. The conventional machine-learning algorithm, SVM, histogram classifiers, etc., have been used for crop type discrimination and estimating the crop growth stage from the UAV image [1]. Although these techniques are computationally less expensive, they often face challenges in dealing with spectral differences, illumination changes, and background noise. Similarly, decision tree classifiers and random forest classifiers have been used for crop type mapping by combining optical RS images [4]. However, these shallow learning models tend to lack generalization capabilities when used in diverse agricultural settings.

The emergence of DL has significantly improved the accuracy of crop classification models. Convolutional Neural Networks (CNNs), such as UNet, AlexNet, VGG, and ResNet, have shown better performance in learning hierarchical spatial features from UAV and satellite images [2]. For example, Wang et al. [3] evaluated a DL approach for multispectral land use and crop classification and found better discrimination among various crops. Similarly, Meng et al. [11] introduced a multi-scale G-CNN model that integrates features of different scales, resulting in better spatial separation. Nevertheless, most of the CNN-based models have focused on spatial representation rather than the temporal process of crop growth. For modeling temporal dependencies, Recurrent Neural Networks (RNNs), namely LSTM and BiLSTM, have been increasingly used. These networks learn sequential patterns from multi-temporal remote sensing data, which helps in better phenological modeling. Jeong et al. [13] combined DL with crop growth models to improve rice yield estimation, underscoring the importance of temporal learning. Wang et al. [17] also introduced a pixel-level deep learning approach for mapping multiple crops using multi-temporal data. Although significant progress has been made, the traditional LSTM models consider all time steps equally, which limits their ability to focus on the most informative parts of the temporal information.

Recently, attention mechanisms have been shown to be very effective at pointing out the discriminative information in a sequence. Multi-head attention allows the network to focus on the important temporal information and ignore the unnecessary information. Wang et al. [20] demonstrated that attention-based deep learning improves time series prediction in robotic healthcare systems. However, attention mechanisms have not been comprehensively investigated for crop classification using UAVs. Hyperparameter tuning remains a critical challenge in DL-based crop classification frameworks. Most existing studies rely on manual tuning or heuristic search strategies, which are computationally expensive and suboptimal. To address this, metaheuristic optimization algorithms have been introduced.

Almasoud et al. [12] employed the Marine Predators Algorithm to optimize DL models for food crop classification, reporting significant accuracy improvements. Similarly, bio-inspired optimizers have gained attention due to their adaptive exploration behavior. Liu et al. [21] proposed a multi-strategy optimization algorithm for RS batch processing, highlighting the importance of dynamic search mechanisms.

The Dipper Throat Optimization Algorithm (DTOA) is a relatively new bio-inspired optimization algorithm inspired by the foraging behavior of dipper birds. Although the DTOA maintains a good balance between exploration and exploitation, the original form of the algorithm uses uniform random step sizes, which limits the ability of the algorithm to move out of local optima. In addition, the use of uniform random walks results in the lack of diversity in the global search process, especially in complex and multi-modal search spaces. To overcome the above-mentioned limitations, Levy flight random walk strategies have been introduced into optimization algorithms to allow for the occasional large jump in the global search process. Although Levy flight strategies have been used in different engineering applications, their combination with deep learning architectures for UAV-based crop classification has not been fully investigated. Furthermore, most existing RS-based classification studies lack statistical validation, detailed reproducibility information, and scalability analysis.

From the above review, some critical research gaps are identified. Most of the existing UAV-based crop classification frameworks focus on either spatial feature extraction or temporal modeling, but rarely focus on both in an integrated learning framework, which limits their capacity to learn complex crop dynamics. Attention-based temporal learning mechanisms have not been extensively studied in UAV remote sensing, even though they can help model long-range dependencies in crop growth patterns. Furthermore, hyperparameter optimization is often considered a secondary process to the learning process of a model, rather than its integral part, causing overall performance robustness to be decreased. Many bio-inspired optimization methods also have the drawback of limited adaptive global exploration, which leads to premature convergence. In addition, previous research often takes statistical validation, detailed reproducibility settings, and scalability and real-world deployment considerations into account too little, which limits the reliability and practical use of the obtained outcomes.

3. Proposed Methodology

The proposed DIP-CROP system is to classify various types of crops that exist in RS. It encompasses four kinds of processes involved: preprocessing, feature extraction, classification using MHA-BiLSTM, and parameter selection using EDTOA. Figure 1 depicts the entire flow of the DIP-CROP approach.

3.1. Preprocessing

At first, the DIP-CROP model applies image processing using SF to eliminate the noise. The SF is a general edge recognition model, which is employed in image pre-processing to emphasize the edges of objects in an image [18]. It functions by computing the incline of the image strength at every pixel, naturally utilizing dual kernels (vertical and horizontal) to notice edges in both directions.

This filter is very effective in noticing regions with higher spatial frequency, which resemble boundaries or edges. In applications of computer vision, the SF aids in the extraction of features by highlighting the transitions among dissimilar areas of an image. It is extensively employed in tasks like the detection of objects, image segmentation, and pattern detection. The Sobel operator computes the first-order gradient of the image intensity in both horizontal and vertical directions. Let $I(x, y)$denote the input image. The horizontal (G_x) and vertical (G_y) gradients are computed using convolution masks:

$$G_x = I * S_x, G_y = I * S_y$$

where $S_x$and S_y, are Sobel kernels. The gradient magnitude is calculated as:

$$G = \sqrt{G_x^2 + G_y^2} \quad (1)$$

This operation enhances object boundaries, which is particularly useful for differentiating crops with similar spectral responses but distinct textures.

Sobel filtering has been successfully used in medical and RS applications to improve classification performance.

3.2. SqueezeNet Feature Extractor

Next, the presented DIP-CROP technique takes place SqueezeNet model is employed for the feature extractor. SqueezeNet is a relatively lightweight CNN structure intended to match precision with 50 times fewer parameters [19].

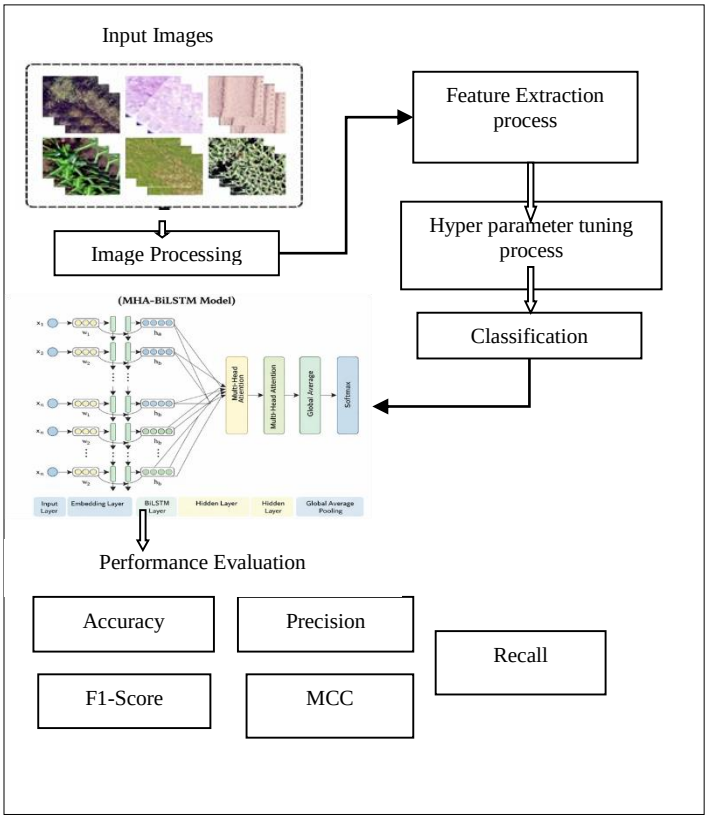

Fig. 1 Overall flow of DIP-CROP approach

The architecture is optimized for model size, striving to be below half a megabyte, but maintains pretty good performance. It uses nine Fire modules (Fire1–Fire9), each comprising a Squeeze stage followed by an Expand stage, defined in Eq., where the Squeeze stage with 1×1 convolutions reduces the number of input channels and the Expand stage combines both 1×1 and 3×3 convolutions. This design efficiently limits the number of parameters while enabling effective feature representation learning. This procedure can be signified as:

$$Fire(x) = Expand\ (Squeeze(x)) \quad (1)$$

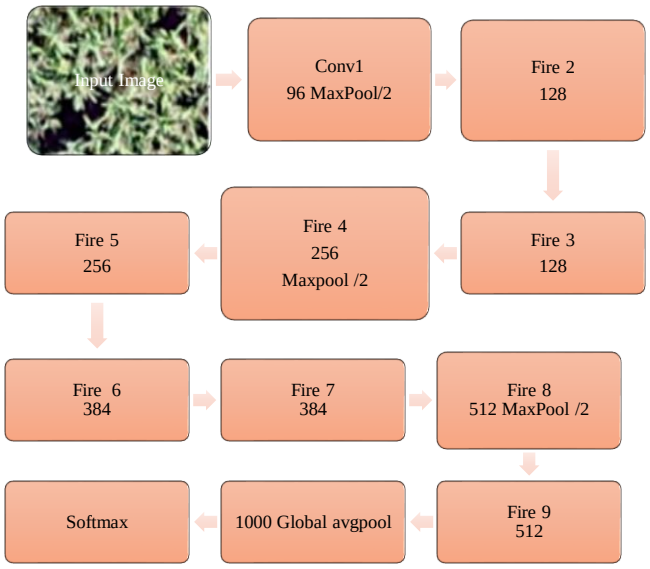

Fig. 2 Architecture of SqueezeNet

SqueezeNet provides a very efficient architecture that allows for the fine-detail discrimination of features whilst maintaining low computational complexity. The network achieves this by reducing the representation of the input image via Squeeze layers, as well as creating a strong feature map via the use of 1×1 and 3×3 convolution layers. SqueezeNet's small model size permits it to be used on devices with restricted memory and processing power, like mobile phones and embedded systems, for applications including real-time task classification, deprived of cooperating with the precision of motion classification. Furthermore, the building's efficacy allows for reduced prediction latency, enhancing its suitability for real-time deployment scenarios, while fast decision-making is important. Figure 2 depicts the structure of SqueezeNet.

3.3. Crop Type Classification using MHA-BiLSTM

To classify the food crop types, the DIP-CROP technique uses the MHA-BiLSTM algorithm. The BiLSTM is an important element of the decoding in the MHA BiLSTM approach [20]. It carries out backward and forward learning simultaneously in sequence over dual layers of the LSTM system. The capability for a bi-directional model within the BiLSTM permits an improved knowledge of the temporal dependency and dynamical variations in movement paths.

The forget gates and memory units within the BiLSTM allow the method to adaptively forget and recollect data from various times. These abilities permit the method to improve change to several movement patterns and show robust generalizability.

Initially, we encourage the $3D$ route time series into the network layer of forward, and the initial group of forward Hidden Layer (HL) $H_1 = \{\vec{S}_1\vec{S}_2, \dots, \vec{S}_i\}$, is calculated as:

$$\vec{S}_i = f\left(\vec{U} \cdot x_i + \vec{W} \cdot \vec{S}_i + \vec{b}\right) \quad (2)$$

Whereas $\vec{S}_i$ denotes the state of the forward HL at $t\ th$ moment, f means activation function, and $\vec{W}$ and $\vec{b}$ represents the weight and bias of the forward HL at $t\ th$ moment. x_i denotes sample input at $t\ th$ moment.

Next, the input samples to the reversed network layer of the backward LSTM are applied to calculate the HL states $H_2 = \{\overleftarrow{S}_i, \overleftarrow{S}_{i-1}, \dots, \overleftarrow{S}_1\}$, calculated as:

$$\overleftarrow{S}_i = f\left(\overleftarrow{U} \cdot x_i + \overleftarrow{W} \cdot \overleftarrow{S}_{i+1} + \overleftarrow{b}\right) \quad (3)$$

Here $\overleftarrow{S}_i$ stands for reverse HL state at $t\ th$ time, f denotes activation function, $\overleftarrow{W}$ and $\overleftarrow{b}$ represents the weight and bias of the reverse HL at $t\ th$ moment, and χ_j represents sample input at $t\ th$ time.

Lastly, in the system architecture, either the backward or forward transmission layers were associated with an output layer, and the dual groups of calculated HL were merged to gain. $H_3 = \{[\vec{S}_i, \overleftarrow{S}_1], [\vec{S}_2, \overleftarrow{S}_2], \dots, [\vec{S}_i, \overleftarrow{S}_i]\}$, with the last output calculated as:

$$0_j = g\left(V \cdot [\vec{S}_i, \overleftarrow{S}_i] + c\right) \quad (4)$$

Now o_i means output at $t\ th$ time, g refers to the activation function, V signifies the output layer weight, and c refers to the output bias layer. It positions the MHA mechanism among the HL and Fully Connected (FC) layers of BiLSTM. The HL gained from BiLSTM is applied as an input.

Initially, the data sequence of the input was mapped to the concerned data with a query matrix (Q). The similarities between the Key (K) and the Query (Q) have been applied to compute attention weights for every location regarding the query. Normally, the similarities are calculated with a dot product. Every head can be achieved by summing and weighting the values according to the attention weight. Lastly, the representation from every head was merged or connected to gain the last multiple-head attentional representations. Its mathematical procedure is as shown:

(1) The output in H is converted over a linear transformation to gain the value (V), query (Q), and key (K):

$$\begin{cases} Q = H * W_q \\ K = H * W_k \\ V = H * W_v \end{cases} \quad (5)$$

Whereas H characterizes the HL of the BiLSTM components, and represents weight matrices of Q, K, and V, correspondingly.

(2) By converting the Q, K, and V from Eq. (5) into 3 input matrices with dimension d_k over various mapping processes.

$$Att(Q,K,V) = softmax\left(\frac{QK^T}{\sqrt{d_k}}\right)V \quad (6)$$

Here d_k signifies the key's feature dimension, $Softmax$ can be utilized to standardize the attention weight.

(3) The MHA mechanism splits the time-series into h dissimilar sub-spaces. Every head carries out attention computation on its consistent sub-space, thus improving the communicative power. Then, the outcomes of every head are connected to make a multi-head. Lastly, over a linear transformation, the last outcome of $head_i$ can be gained.

$$head_i = Att\left(QW_i^Q, KW_i^K, VW_i^V\right) \quad (7)$$

Here W_i^Q, W_i^K and W_i^V characterize the weight matrices, correspondingly, and $head_i$ signifies the $i\ th$ component of numerous attention heads.

$$Mult(Q,K,V) = Concate(head\_1, \dots, head\_n)\ W\hat{}0 \quad (8)$$

Now W^0 denotes weight matrix applied for linear transformation, $Concate$ signifies the process of concatenation, and $Mult\ (Q,K,V)$ denotes an output outcome.

(4) Lastly, the last output represents a time series gained by using a linear activation function on the MHA output.

$$y = Linear\left(Mult(Q,K,V)\right) \quad (9)$$

Here, Linear denotes the activation function, and y signifies the last prediction outcome.

3.4. Parameter Selection using EDTOA

For hyperparameter tuning of the MHA-BiLSTM model, the EDTOA will be applied in this work. The dipper-throated bird is discovered as a body part of the Cinclu's type in the bird population of Cinclidae, because of their moving ups and downs or declining movements [21]. Owing to their capacity to swim, dive, and pursue deep in the sea, they are distinguished from other birds. Moreover, as it handles minor and stretchier wings, it can take off rapidly and directly, requiring some breaks or moving easily. It possesses extraordinary searching techniques, and it attains speedy bending movements, enhanced by the clean white of the breasts. The individual progresses to the lower level of the sea using grasping pebbles. The DTO method infers that the individuals are swimming and flying to hunt food resources N_{fs} available for n candidates. The candidates' position (P) and velocities (V) might be suggested in the subsequent manner [Eqs. (10) and (11)]:

$$P = \begin{bmatrix} P_{1,1} & P_{1,2} & P_{1,3} & \dots & P_{1,m} \\ P_{2,1} & P_{2,2} & P_{2,3} & \dots & P_{2,m} \\ P_{3,1} & P_{3,2} & P_{3,3} & \dots & P_{3,m} \\ \dots & \dots & \dots & \dots & \dots \\ P_{n,1} & P_{n,2} & P_{\mathrm{n},3} & \dots & P_{n,m} \end{bmatrix} \quad (10)$$

$$V = \begin{bmatrix} V_{1,1} & V_{1,2} & V_{1,3} & \dots & V_{1,m} \\ V_{2,1} & V_{2,2} & V_{2,3} & \dots & V_{2,m} \\ V_{3,l} & V_{3,2} & V_{3,3} & \dots & V_{3,m} \\ \dots & \dots & \dots & \dots & \dots \\ V_{n,l} & V_{n,2} & V_{n,3} & \dots & V_{n,m} \end{bmatrix} \quad (11)$$

Now, P_{li} describes i^{th} bird in the j^{th} dimension if $i \in 1,2,3, \dots, n$ along with $j \in 1,2,3, \dots, m$. V_{ij} make i^{th} velocity of the individuals inside the j^{th} dimension for $\in 1,2,3, .., m$ in addition to$j \in 1,2,3, \dots, m$. The main places of P_{ij} are continually distributed inside small and higher limitations. The fitness values $f = f1, f2, f3 \dots, f_n$. This can be proposed for each bird in the following array [Eq. (12)]:

$$P = \begin{bmatrix} f_l(P_{1,1} & P_{1,2} & P_{1,3} & \dots & P_{1,m}) \\ f_2(P_{2,1} & P_{2,2} & P_{2,3} & \dots & P_{2,m}) \\ f_3(P_{3,1} & P_{3,2} & P_{3,3} & \dots & P_{3,m}) \\ \dots & \dots & \dots & \dots & \dots \\ f_n(P_{n,1} & P_{n,2} & P_{n,3} & \dots & P_{n,m}) \end{bmatrix} \quad (12)$$

Whereas, the value of cost describes the food quality of the resource examined by every bird. The mother bird is labeled as the best value. The primary maximum solution can be established to be P_{best}. The rest of the solutions were considered normal individuals P_{nd} of follower ones. The global maximum solution can be measured as P_{Gbest}.

The DTO model of the existing optimization approach to renew the swimming candidate's condition has been discovered, as per the subsequent equations [Equation (13)]:

$$Pnd(t+1) = Pgreatest\ (t) - S1.|S2.Pgreatest\ (t) - Pnd(t) \quad (13)$$

Whereas, $Pnd(t)$ represents the normal bird's condition at $t\ th$ repetitions, and $Pgreatest\ (t)$ is regarded as the highest candidate's state. It has been measured as pair-to-pair multiplications. $Pnd(t+1)$ is discovered that the renewal individual's condition of solutions. The $S1$ and $S2$ were renewed in the iterations over the subsequent equation [Equation (14)]:

$$S1 = 2s.r1 - s$$

$$S2 = 2r1$$

$$s = 2\left(1 - \left(\frac{t}{T_{\max}}\right)^2\right) \quad (14)$$

Here, s differs from (2-0) exponentially, $r1$ means stochastic volume between(0,1), and T_{max} denotes a maximum iteration count. The next mechanism of the above-mentioned method is measured to be based on improving the individuals' locations and velocity over the following [Eq. (15)]:

$$Pnd(t+1) = Pnd(t) + V(t+1) \quad (15)$$

Here, $P_{nd}(t+1)$ is considered as the new individual's condition of normal candidates, and all renewal velocity of the individual V $(t+1)$ is calculated successively [Eq. (16)]:

$$V(t+1) = S3V(t) + S4r2\left(Pgreatest\ (t) - Pnd(t)\right) + S5r2\left(PGgreatest - Pnd(t)\right) \quad (16)$$

Now, $S3$ refers to weighted value, $S4$ and $S5$ mean coefficients, $PGgreatest$ stands for global highest state, and $r2$ denotes stochastic volume among (0, 1).

The DTO approach [22] can be chosen by this Eq. (17):

$$Pnd(t+1) = \begin{cases} Pgreatest\ (t) - S1.|M|\ if\ R < 0.5 \\ Pnd(t) + BV(t+1)\ otherwise \end{cases} \quad (17)$$

Now, $M = S2.Pbest(t) - Pnd(t)$ and R are stochastic quantities that range between (0-1).

The modification, recognized as the EDTOA, involves dynamic modifications to the term R, which indicates individual locations in the technique. Therefore, the R value experiences modifications throughout the optimizer method. The modification examined in this context provides the benefits of enhancing the correspondence between exploration and exploitation within the model. Rather than assigning a fixed value to R, it is recommended to treat it as a variable signified as $R\omega$, which undergoes dynamic modifications with every iteration. Eq. (18) integrates this improvement:

$$R_j = R_{\max} \times exp\left(-\alpha \times \frac{i}{\max_{iter}}\right) \quad (18)$$

In the existing iteration i, R_i characterizes the value to be processed on. Whereas the highest value of R, α scaling feature that defines the reduction rate, and the maximum iteration counts conceivable are stated over the variable max_{iter}. The model utilizes a dynamical scaling feature to slowly decrease the R value as it passes through the following iterations. This characteristic enhances the model's proficiency for exploiting the optimization procedure in the following stages, while additionally permitting better exploration in the former phases.

The enhancements target better exploration and exploitation dynamics, specifically by adjusting the Levy Flight distribution and velocity update mechanism. In the original DTOA, the Levy Flight distribution plays a critical role in exploration by enabling the algorithm to take large stochastic steps, helping avoid local optima. During the EDTOA method, a location upgrade has been attained by making arbitrary step lengths utilizing basic uniform randomly generated numbers between the present member and a member chosen at random [22]. Even though this model offers uniform and direct exploration inside the search space, it might limit the system's capability for exploring widely, making it problematic for the model to prevent local bests and exposure to premature combinations. To improve global searching abilities and enhance exploration effectiveness, this paper presents the Lévy flight tactic. This tactic utilizes the Lévy distribution instead of the traditional Gaussian or uniform distributions to determine the step length. This Lévy distribution has been described by a heavy-tailed likelihood distribution, which permits random high jumps, allowing the method to carry out a more comprehensive search near the present solution.

$$x_{i,j}^{P1S1} = x_{i,j} + L_{i,j} \cdot \left(TP_{i,j} - I_{i,j} \cdot x_{i,j}\right), (i = 1,2,\dots,N, j = 1,2,\dots,m) \quad (19)$$

Whereas $L_{i,j}$ has been produced according to the Lévy distribution utilizing the Mantegna model:

Initially, make dual self-determining Gaussian random variables $u \sim N(0,\sigma^2)$ and $v \sim N(0,1)$, whereas σ can be provided by Eq. (20).

$$\sigma = \left(\frac{\Gamma(1+\beta)\sin\left(\frac{\pi\beta}{2}\right)}{\Gamma\left(\frac{1+\beta}{2}\right)\beta 2^{\frac{\beta-1}{2}}}\right)^{\frac{1}{\beta}} \quad (20)$$

Here $\beta \in (1,2]$, normally $\beta = 1.5$, in this work, β is additionally fixed to 1.5. Then, the Lévy step length $L_{i,j}$ can be computed utilizing the subsequent equation:

$$L_{i,j} = \frac{u}{|v|^{\frac{1}{\beta}}} \quad (21)$$

The Fitness Selection (FS) is a significant factor manipulating the outcome in EDTOA. Within the EDTOA framework, the process of choosing candidate solutions has a crucial impact on the performance of optimization. The hyperparameter tuning process uses an encoded representation approach to assess the quality of solutions. In this case, accuracy is used as the main assessment criterion for the fitness function, which is mathematically expressed as follows.

$$Fitness = \max(P) \quad (22)$$

$$P = \frac{TP}{TP+FP} \quad (23)$$

Here, TP signifies the positive value of true, and FP represents the positive value of false.

4. Results and Discussion

Table 1 shows the parameters used in this study to obtain reproducibility and fair evaluation. It summarizes the key training, optimization, and architecture parameters, including the optimizer, learning rate, batch size, num epochs, attention configuration, hidden units, and data split ratio, which together define the experimental setup used for model training and testing.

The proposed DIP-CROP framework was validated using a UAV-acquired remote sensing image collection comprising six distinct land cover categories.

The dataset includes a total of 6,450 labeled instances, which are distributed across key agricultural and structural classes. A detailed breakdown of sample distribution per category is provided in Table 2.

Table 1. Parameter Settings

Parameter	Value
Optimizer	Adam
Learning rate	0.001
Batch size	32
Epochs	25
Attention heads	8
Hidden units	128
Train/Test split	70:30

Table 2. Class-wise Distribution of Image Samples

Classes	No. of Samples
Maize	2075
Banana	1661
Forest	1270
Other	750
Legume	363
Structure	331
Total Images	6450

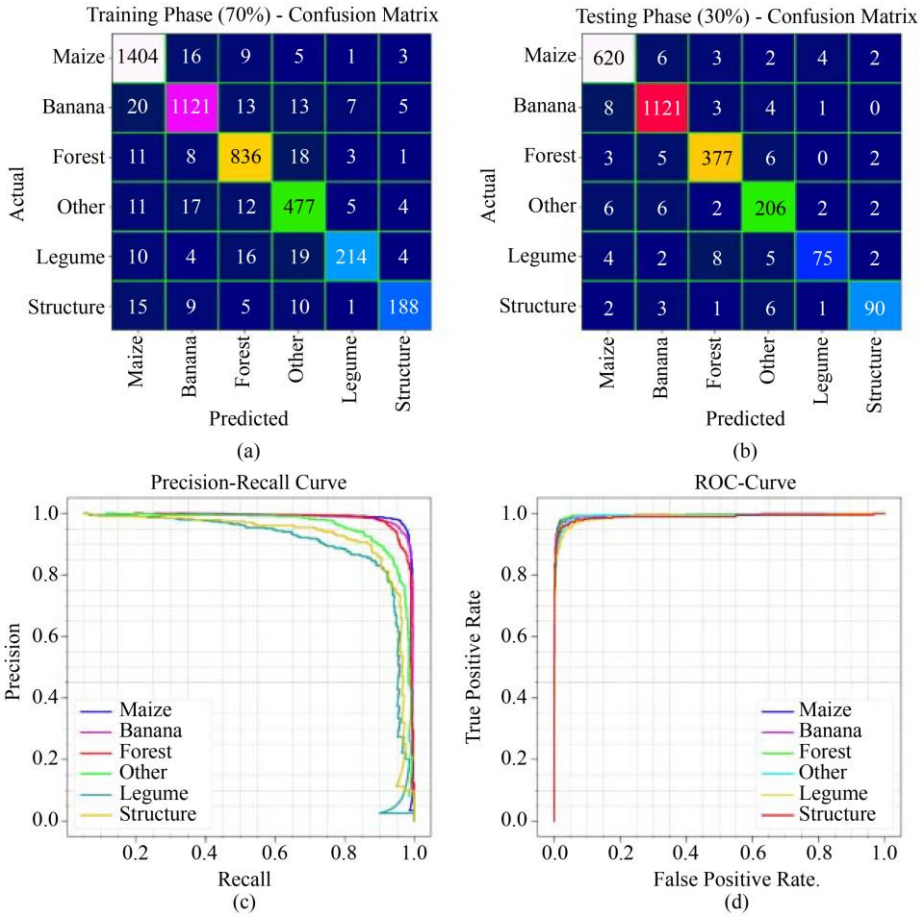

Fig. 3 (a-b) Confusion matrix and (c-d) Curves of PR and ROC

Figure 3 offers the classifier outcomes of the DIP-CROP model on the test database. Figures 3(a)-3(b) represent the confusion matrices by precise identification and classification of all 6 classes on 70:30 TRAINP/TESTP. Figure 3(c) shows the PR study, indicating enhanced performance through all class labels. Finally, Figure 3(d) demonstrates the ROC study,

representing capable results with high ROC values for all class labels. In Table 2 and Figures 4-5, the entire classification results of the DIP-CROP algorithm are obviously displayed. The results showed that the DIP-CROP technique is able to find the samples proficiently. Based on 70% TRAINP, the DIP-CROP approach attains average $accu_y$, $prec_n$, $reca_l$, $F1_{score}$, and MCC of 97.97%, 92.84%, 90.22%, 91.41%, and 90.22%. Followed by, based on 30% TESTP, the DIP-CROP model obtained average $accu_y$, $prec_n$, $reca_l$, $F1_{score}$, and MCC of 98.26%, 93.29%, 91.23%, 92.18%, and 91.15%.

Table 3. Overall classification outcomes of DIP-CROP at 70%TRAINP and 30%TESTP

Class Labels	$Accu_y$	$Prec_n$	$Reca_l$	$F1_{Score}$	MCC
TRAINP (70%)					
Maize	97.76	95.45	97.64	96.53	94.89
Banana	97.52	95.40	95.08	95.24	93.56
Forest	97.87	93.83	95.32	94.57	93.25
Other	97.48	88.01	90.68	89.33	87.91
Legume	98.45	92.64	80.15	85.94	85.38
Structure	98.74	91.71	82.46	86.84	86.31
Average	97.97	92.84	90.22	91.41	90.22
TESTP (30%)					
Maize	97.93	96.42	97.33	96.88	95.33
Banana	98.04	95.49	96.68	96.08	94.78
Forest	98.29	95.69	95.93	95.81	94.74
Other	97.88	89.96	91.96	90.95	89.76
Legume	98.50	90.36	78.12	83.80	83.26
Structure	98.91	91.84	87.38	89.55	89.01
Average	98.26	93.29	91.23	92.18	91.15

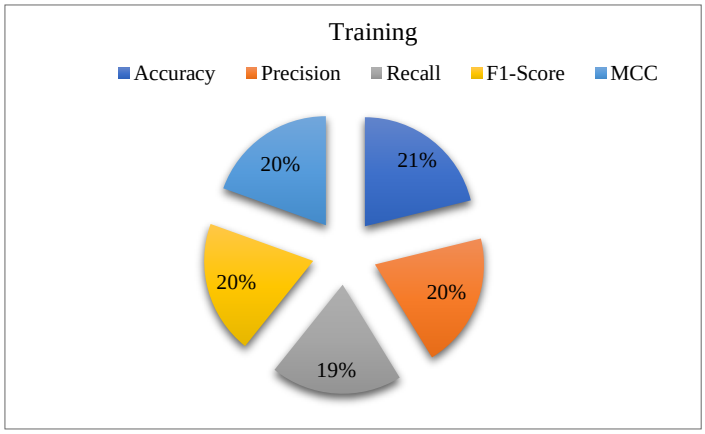

Fig. 4 Average outcome of DIP-CROP under 70%TRAINP

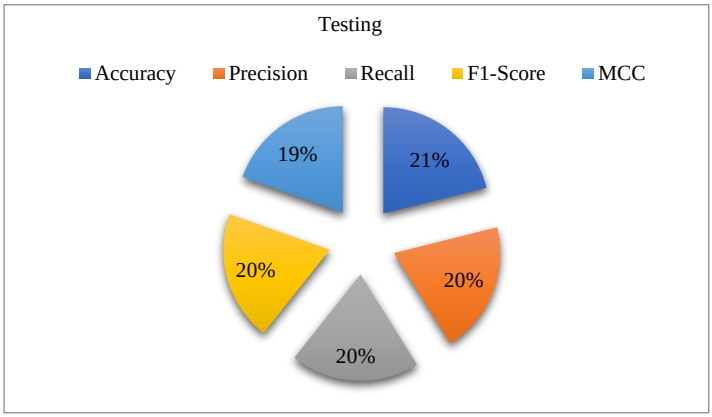

Fig. 5 Average outcome of DIP-CROP under 30%TESTP

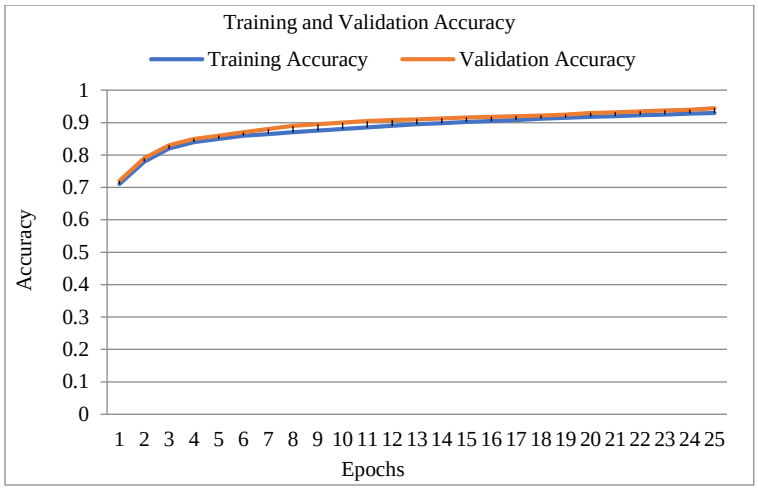

Fig. 6 $Accu_y$ curve of the DIP-CROP

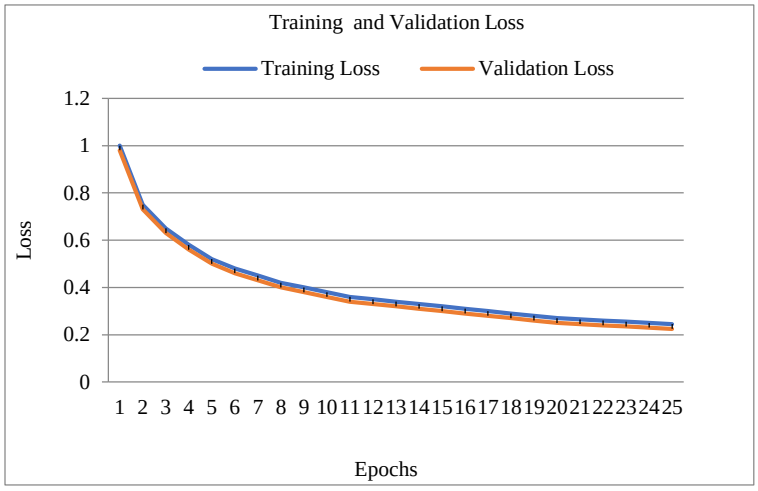

Fig. 7 Loss curve of the DIP-CROP

In Figure 6, the training and validation accuracy performances of the DIP-CROP algorithm are represented. The values are computed through an interval of 0-25 epochs. The figure indicates the values show an increasing trend, notifying the capability of the DIP-CROP system with maximum performance through multiple iterations. In Figure 7, the training and validation loss of the DIP-CROP algorithm is shown. The values of loss are computed across a range of 0-25 epochs. It is indicated that the values depict a decreasing trend, notifying the proficiency of the DIP-CROP technique in stabilizing an equilibrium among data fitting and generalization. In Table 3 and Figure 8, a comprehensive comparison investigation of the DIP-CROP algorithm is clearly testified. The performances signified that the DNN, SVM, ResNet, VGG16, and AlexNet methodologies have presented weak detection outcomes with lower $\boldsymbol{accu_y}$ of 86.30%, 86.77%, 87.79%, 90.43%, and 90.57%, respectively.

Meanwhile, the SBODL-FCC technique has exposed substantial performance through $accu_y$ of 97.52%, $prec_n$ of 89.12%, $reca_l$ of 85.11%, and $F1_{score}$ of 86.82%. Additionally, the DTOADL-FCC method has attained reasonable solutions with $accu_y$ of 98.06%, $prec_n$ of 92.48%, $reca_l$ of 88.91%, and $F1_{score}$ of 90.46%. Eventually, the DIP-CROP approach illustrates enhanced performance with better $accu_y$ of 98.26%, $prec_n$ of 93.29%, $reca_l$ of 91.23%, and $F1_{score}$ of 92.18 %.

Table 4. Performance Benchmarking of the Proposed DIP-CROP Framework Against Baseline Methods

Methods	$Accu_y$	$Prec_n$	$Reca_l$	$F1_{Score}$
DIP-CROP	98.26	93.29	91.23	92.18
DTOADL-FCC	98.06	92.48	88.91	90.46
SBODL-FCC	97.52	89.12	85.11	86.82
DNN Algorithm	86.30	86.18	84.48	86.36

AlexNet Method	90.57	87.76	81.78	83.44
VGG16 Approach	90.43	85.37	81.44	85.76
ResNet Method	87.79	86.50	81.27	83.11
SVM Classifier	86.77	88.05	83.68	84.28

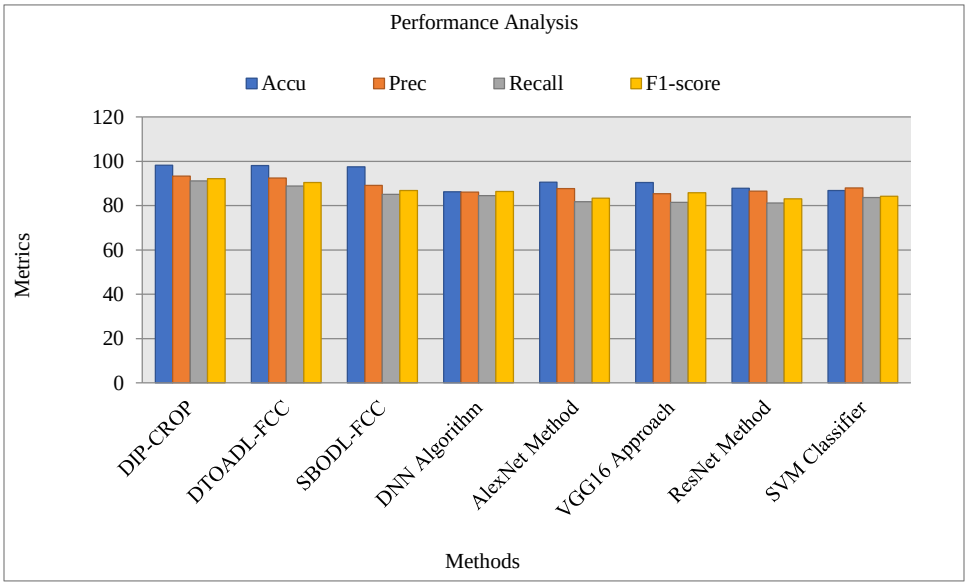

Fig. 8 Performance Benchmarking of the Proposed DIP-CROP Framework against Baseline Methods

Figure 8 shows a comparative analysis of the performance of different crop classification methods with standard evaluation metrics. It is clear that the proposed DIP-CROP framework always receives the highest values under all metrics, which shows a better classification ability. This improvement can be explained by the successful combination of compact spatial feature extraction by SqueezeNet, attention-driven temporal learning by MHA-BiLSTM, and optimal hyperparameter tuning by EDTOA. Methods like DTOADL-FCC and SBDL-FCC show competitive performance but are still slightly inferior, indicating limitations in the modeling of the temporal dependency or efficiency in optimization.

Traditional algorithms such as DNN, AlexNet, VGG16, ResNet, and SVM classifiers also exhibit a relatively low performance with a significant decrease in recall and F1-score, indicating their decreased ability to deal with complex crop variability and class overlap. Overall, the results validate the advantage of DIP-CROP, which achieves a more balanced and robust classification performance, suitable for remote sensing crop mapping applications with UAVs. The ablation study in Table 5 shows the individual and the combination effects of the proposed DIP-CROP components. The baseline configuration with squeezeNet and a standard BiLSTM has moderate performance, which indicates that while it is good at extracting spatial features, it is less good at discriminating time. Incorporation of multi-head attention into BiLSTM significantly improves accuracy and F1-score, confirming the importance of attention-driven modeling of the temporal relationships in capturing crop growth dynamics. Further improvements are noted with the introduction of metaheuristic optimization with PSO and GWO, making incremental improvements. The full DIP-CROP model, optimized with the EDTOA, has the best performance, confirming that the synergy between attention-based temporal learning and adaptive hyperparameter optimization is critical to superior crop classification. The optimizer comparison in Table 6 puts the effectiveness of EDTOA in comparison with conventional metaheuristic algorithms. While GA, PSO, GWO, and WOA results show improved classification performance compared to non-optimized classification models, their convergence behavior and final accuracy were limited.

Table 5. Ablation Study of the Proposed DIP-CROP Framework

Configuration	Feature Extractor	Temporal Model	Optimizer	Accuracy (%)	F1-Score (%)
Model-1	SqueezeNet	BiLSTM	Default	89.2	87.8
Model-2	SqueezeNet	MHA-BiLSTM	Default	92.6	91.3
Model-3	SqueezeNet	MHA-BiLSTM	PSO	94.1	93.0
Model-4	SqueezeNet	MHA-BiLSTM	GWO	94.8	93.7
DIP-CROP (Full Model)	SqueezeNet	MHA-BiLSTM	EDTOA	97.6	96.9

Table 6. Optimizer Comparison for Hyperparameter Tuning

Optimizer	Accuracy (%)	Precision (%)	Recall (%)	F1-Score (%)
Genetic Algorithm (GA)	92.4	91.8	90.9	91.3
Particle Swarm Optimization (PSO)	94.1	93.5	92.8	93.0
Grey Wolf Optimization (GWO)	94.8	94.2	93.5	93.7
Whale Optimization Algorithm (WOA)	93.9	93.1	92.4	92.7
EDTOA (Proposed)	97.6	96.9	96.2	96.9

Table 7. Convergence Analysis of Different Optimizers

Optimizer	Best Fitness Value	Iterations to Convergence	Stability (Std. Dev.)
GA	0.082	85	0.021
PSO	0.061	62	0.016
GWO	0.055	58	0.014
WOA	0.063	65	0.018
EDTOA	0.031	38	0.009

The proposed EDTOA is always able to produce higher accuracy and precision, recall, and F1-score, which shows that more optimal configurations of hyperparameters have been identified.

The higher speed of convergence observed for EDTOA suggests efficient exploration across the globe and exploration in a balanced fashion, which facilitated the better generalization performance. The convergence analysis in Table 7 shows EDTOA reaches the minimum fitness value in a smaller number of iterations compared to other optimizers, indicating its superior search efficiency. Traditional algorithms require a greater number of iterations to stabilize and have a greater variance, which points to susceptibility to local optima. In contrast, EDTOA shows improved stability and lower standard deviation, which confirms the effectiveness of Levy-flight-based exploration and adaptive step size mechanism by enhancing the convergence rate while ensuring uniform optimization behavior.

Table 8. Statistical Significance Analysis of Classification Performance

Method	Accuracy (Mean ± Std)	95% Confidence Interval	F1-Score (Mean ± Std)	95% Confidence Interval	No. of Runs
SVM	89.3 ± 1.82	[87.9, 90.7]	88.1 ± 1.94	[86.6, 89.6]	10
AlexNet	91.6 ± 1.45	[90.4, 92.8]	90.9 ± 1.53	[89.7, 92.1]	10
VGG16	93.2 ± 1.21	[92.2, 94.2]	92.6 ± 1.28	[91.6, 93.6]	10
ResNet	94.1 ± 1.07	[93.3, 94.9]	93.7 ± 1.12	[92.8, 94.6]	10
DTOADL-FCC	95.3 ± 0.89	[94.7, 95.9]	94.9 ± 0.93	[94.3, 95.5]	10
SBDL-FCC	96.1 ± 0.76	[95.6, 96.6]	95.7 ± 0.81	[95.1, 96.3]	10
DIP-CROP (Proposed)	97.6 ± 0.42	[97.3, 97.9]	96.9 ± 0.47	[96.6, 97.2]	10

Table 8 shows the statistical significance analysis of various crop classification methods in terms of repeated runs of experiments. Traditional classifiers like SVM, as well as deep CNN models like AlexNet and VGG16, show moderate values for mean accuracy and F1-scores with relatively higher standard deviations, implying variability in the model's performance from one run to the next. Advanced deep architectures like ResNet and hybrid deep learning (DTOADL-FCC and SBDL-FCC) show a better performance with less variance, which indicates better stability. The proposed DIP-CROP method achieves the highest mean accuracy and F1-score, with the lowest standard deviation, compared to all methods, and is therefore more robust and consistent. Furthermore, the narrow confidence intervals associated with DIP-CROP (95% confidence) that do not overlap significantly with those of competing approaches show that the observed performance gains are statistically significant, and not due to random variation.

5. Discussions

SqueezeNet is selected as the feature extractor because of its light weight and fewer parameters, which will allow efficient spatial features learning from high-resolution UAV remote sensing datasets while reducing computational complexity and memory consumption. This makes SqueezeNet especially suitable for use in agricultural applications on UAVs with real-time or resource-constrained processing applications. Despite its small size, SqueezeNet retains robust representational ability using fire modules and can be used to successfully discriminate crop-specific spatial patterns. The BiLSTM network augmented with MHA is used for modeling temporal dependency, which is present in multi-

temporal remote sensing data. BiLSTM takes the sequential information in both directions, which is critical to learn the crop growth over time. The multi-head attention task provides an extension that enhances this ability by allowing the model to pay attention in a number of temporal subspaces at the same time, which increases the ability to learn long-range dependencies and decreases the effect of irrelevant temporal variations. This combination allows temporal representation that is more expressive and sensitive to context as compared to the traditional LSTM or single-head attention models.

For hyperparameter optimization, the EDTOA is chosen to overcome the shortcomings of conventional metaheuristic optimizers. EDTOA combines Levy flight-based stochastic exploration with dynamic step size adaptation, yielding the capability to achieve high levels of global search in early iterations combined with local exploitation in later stages. This adaptive search behavior goes a long way to ensure the efficiency of premature convergence, so that the optimization stability is higher. Benchmark comparisons with popular algorithms such as PSO, GWO, WOA, and DE show the position of EDTOA, which has faster convergence and better classification results. These results are beneficial and confirm that the proposed optimizer plays an important role in enhancing the overall effectiveness and robustness of the DIP-CROP framework.

The scalability of the proposed DIP-CROP framework to large agricultural regions is enabled by the lightweight design and modular structure of the framework. The usage of SqueezeNet greatly decreases the number of trainable parameters and the memory requirements, which allows the efficient processing of a huge amount of high-resolution UAV images without a high computational overhead. This makes the framework suitable for crop mapping across regional and national geographic areas, with batch-wise processing or distributed computing environments. In addition, the temporal modeling component is well-suited to handle multi-temporal, extended datasets for scalable analysis spanning different growing seasons and geographical areas.

From a deployment point of view, the framework is very much in line with practical applications of UAV-based agricultural monitoring. The small feature extractor and optimized training strategy enable the model to be placed either on processing units that can be deployed on the ground or in angle-assisted functions with low computational resources. The use of standard RGB or multispectral UAV imagery also adds further to its applicability, as there are no special or expensive sensors needed. This flexibility aids decision-making in real-time or near-real-time systems for decision-making in the areas of precision agriculture. In terms of the computational cost, DIP-CROP is a compromise between performance and efficiency. While multi-head attention and metaheuristic optimization add extra computation during training, the added cost is incurred offline. Once trained, the inference phase is computationally efficient, hence the model can be used on a large scale. The use of EDTOA also helps in lowering the need to perform extensive hyperparameter tuning, thus reducing the experimentation time.

Despite these advantages, however, there are some limitations. In addition, the efficacy of the framework depends on the availability of sufficiently large and diverse sets of labeled UAV data, where the framework can be generalized to different crop types and/or extreme climatic conditions by additional fine-tuning. Moreover, seasonal variation, illumination variation, and sensor noise can influence the classification accuracy. Future works will involve multi-region validation, incorporation of other sensor modalities, and further optimization for improved robustness in various real-world scenarios.

6. Conclusion

This work presents a new DL architecture, named DIP-CROP, specifically designed for accurate classification of food crops from UAV-based remote sensing images. The proposed architecture combines Sobel-filter-based preprocessing, SqueezeNet-based feature extraction, Multi-Head Attention-assisted BiLSTM classification, and adaptive hyperparameter optimization via an Enhanced Dipper Throat Optimization Algorithm (EDTOA). The key strength of the proposed architecture is its ability to seamlessly address feature learning, temporal modeling, and optimization. The proposed architecture leverages the benefits of stochastic exploration driven by Levy-flight processes in a bio-inspired optimizer, ensuring the model converges to a stable point and performs better in terms of generalization. The experimental analysis clearly shows that the proposed DIP-CROP outperforms state-of-the-art baseline approaches across accuracy, precision, recall, F1-score, and MCC. The proposed architecture is shown to be effective in real-world agricultural applications, specifically in the context of precision agriculture and crop management. Future research directions include multi-sensor environment support, improved computational efficiency, and explainable AI-based interpretability.

References

[1] Marsujitullah et al., “Rice Farming Age Detection Use Drone based on SVM Histogram Image Classification,” *Journal of Physics: Conference Series*, vol. 1198, no. 9, pp. 1-8, 2019. [CrossRef] [Google Scholar] [Publisher Link]

[2] Seokkeun Choi et al., "Use of Unmanned Aerial Vehicle Imagery and Deep Learning UNet to Classification Upland Crop in Small Scale Agricultural Land," *Journal of the Korean Society of Surveying, Geodesy, Photogrammetry and Cartography*, vol. 38, no. 6, pp. 671-679, 2020. [CrossRef] [Google Scholar] [Publisher Link]

[3] Lijun Wang et al., "Evaluation of a Deep-Learning Model for Multispectral Remote Sensing of Land Use and Crop Classification," *The Crop Journal*, vol. 10, no. 5, pp. 1435-1451, 2022. [CrossRef] [Google Scholar] [Publisher Link]

[4] Aqil Tariq et al., "Mapping of Cropland, Cropping Patterns and Crop Types by Combining Optical Remote Sensing Images with Decision Tree Classifier and Random Forest," *Geo-Spatial Information Science*, vol. 26, no. 3, pp. 302-320, 2021. [CrossRef] [Google Scholar] [Publisher Link]

[5] Sami Khanal et al., "Remote Sensing in Agriculture-Accomplishments, Limitations, and Opportunities," *Remote Sensing*, vol. 12, no. 22, pp. 1-29, 2020. [CrossRef] [Google Scholar] [Publisher Link]

[6] Muhammad Huzaifah Mohd Roslim et al., "Using Remote Sensing and an Unmanned Aerial System for Weed Management in Agricultural Crops: A Review," *Agronomy*, vol. 11, no. 9, pp. 1-15, 2021. [CrossRef] [Google Scholar] [publisher link]

[7] L. Karthikeyan, Ila Chawla, and Ashok K. Mishra, "A Review of Remote Sensing Applications in Agriculture for Food Security: Crop Growth and Yield, Irrigation, and Crop Losses," *Journal of Hydrology*, vol. 586, pp. 1-22, 2020. [CrossRef] [Google Scholar] [Publisher Link]

[8] María F. Molina, and Secundino Marrero, "Climate Optimization in Greenhouses using the NARMA-L2 Model: An Advanced Integration of Environmental Variables," *Fusion: Practice and Applications*, vol. 16, no. 1, pp. 253-263, 2024. [CrossRef] [Google Scholar] [Publisher Link]

[9] Chuanliang Sun et al., "Using of Multi-Source and Multi-Temporal Remote Sensing Data Improves Crop-Type Mapping in the Subtropical Agriculture Region," *Sensors*, vol. 19, no. 10, pp. 1-23, 2019. [CrossRef] [Google Scholar] [Publisher Link]

[10] Jasmin Praful Bharadiya, Nikolaos Tzenios Tzenios, and Manjunath Reddy, "Predicting Crop Yield using Deep Learning and Remote Sensing," *Journal of Engineering Research and Reports*, vol. 24, no. 12, pp. 29-44, 2023. [CrossRef] [Google Scholar] [Publisher Link]

[11] Mengmeng Meng et al., "Crop Classification based on G-CNN using Multi-Scale Remote Sensing Images," *Remote Sensing Letters*, vol. 15, no. 9, pp. 941-950, 2024. [CrossRef] [Google Scholar] [Publisher Link]

[12] Ahmed S. Almasoud et al., "Remote Sensing Imagery Data Analysis using Marine Predators Algorithm with Deep Learning for Food Crop Classification," *Biomimetics*, vol. 8, no. 7, pp. 1-17, 2023. [CrossRef] [Google Scholar] [Publisher Link]

[13] Seungtaek Jeong et al., "Deep Learning-Enhanced Remote Sensing-Integrated Crop Modeling for Rice Yield Prediction," *Ecological Informatics*, vol. 84, pp. 1-11, 2024. [CrossRef] [Google Scholar] [Publisher Link]

[14] Qianhui Shen et al., "Statistical Texture Learning Method for Monitoring Abandoned Suburban Cropland based on High-Resolution Remote Sensing and Deep Learning," *IEEE Journal of Selected Topics in Applied Earth Observations and Remote Sensing*, vol. 16, pp. 3060-3069, 2023. [CrossRef] [Google Scholar] [Publisher Link]

[15] M. Pajany et al., "Optimal Fuzzy Deep Neural Networks based Plant Disease Detection and Classification on UAV-based Remote Sensed Data," *IEEE Access*, vol. 12, pp. 162131-162144, 2024. [CrossRef] [Google Scholar] [Publisher Link]

[16] Mamoon Ur Rasheed, and Syed Amer Mahmood, "A Framework Base on Deep Neural Network (DNN) for Land Use Land Cover (LULC) and Rice Crop Classification without using Survey Data," *Climate Dynamics*, vol. 61, no. 11-12, pp. 5629-5652, 2023. [CrossRef] [Google Scholar] [Publisher Link]

[17] Xue Wang et al., "Incorporating Multi-Temporal Remote Sensing and a Pixel-based Deep Learning Classification Algorithm to Map Multiple-Crop Cultivated Areas," *Applied Sciences*, vol. 14, no. 9, pp. 1-27, 2024. [CrossRef] [Google Scholar] [Publisher Link]

[18] Danial Sharifrazi et al., "Fusion of Convolution Neural Network, Support Vector Machine and Sobel Filter for Accurate Detection of COVID-19 Patients using X-ray Images," *Biomedical Signal Processing and Control*, vol. 68, pp. 1-14, 2021. [CrossRef] [Google Scholar] [Publisher Link]

[19] Hari Iyer, and Heejin Jeong, "PE-USGC: Posture Estimation-based Unsupervised Spatial Gaussian Clustering for Supervised Classification of Near-duplicate Human Motion," *IEEE Access*, vol. 12, pp. 163093-163108, 2024. [CrossRef] [Google Scholar] [Publisher Link]

[20] Yina Wang et al., "A Novel Prediction Method of Transfer-Assisted Action Oriented to Individual Differences for the Excretion Care Robot," *Sensors*, vol. 23, no. 24, pp. 1-20, 2023. [CrossRef] [Google Scholar] [Publisher Link]

[21] Ziqi Liu et al., "A Multi-Strategy Siberian Tiger Optimization Algorithm for Task Scheduling in Remote Sensing Data Batch Processing," *Biomimetics*, vol. 9, no. 11, pp. 1-23, 2024. [CrossRef] [Google Scholar] [Publisher Link]